Laboratory studies on the optical, physical, and chemical properties of fresh and aged biomass burning aerosols

Zheng Yang[1], Qiaoqiao Wang[1], Qiyuan Wang[2], Nan Ma[1], Jie Tian[2], Yaqing Zhou[1], Ge Xu[3], Miao Gao[3], Xiaoxian Zhou[1], Yang Zhang[2], Weikang Ran[2], Ning Yang[1], Jiangchuan Tao[1], Juan Hong[1], Yunfei Wu[4], Junji Cao[4], Hang Su[4], Yafang Cheng[5]

[1]Guangdong-Hongkong-Macau Joint Laboratory of Collaborative Innovation for Environmental Quality, Institute for Environmental and Climate Research, College of Environment and Climate, Jinan University, Guangzhou 511443, China

[2]State Key Laboratory of Loess and Quaternary Geology, Institute of Earth Environment, Chinese Academy of Sciences, Xi'an 710061, China

[3]Xi'an Institute for Innovative Earth Environment Research, Xi'an 710061, China

[4]Institute of Atmospheric Physics, Chinses Academy of Sciences, Beijing 100029, China

[5]Minerva Independent Research Group, Max Planck Institute for Chemistry, Mainz 55128, Germany

Correspondence to: Qiaoqiao Wang (qwang@jnu.edu.cn) and Qiyuan Wang (wangqy@ieecas.cn)

Abstract. Atmospheric brown carbon (BrC) plays a significant role in global warming, yet the evolution of its optical properties during aging remains poorly understood, leading to substantial uncertainties in its climate effects. In this study, we investigate the aging process of BrC and its driving factors using laboratory-generated biomass burning emissions, including four types of straw and one type of wood. Upon OH oxidation, there exists a large increase in OA fraction after 2-day aging, followed by a minor increase during aging to 7 days. The particle growth is dominated by the change in OA content and thus shows a similar trend during aging. The mass absorption efficiency (MAE) of fresh BrC measured at 370 nm is 2.1–5.7 m^2 g^{-1}. A sharp decline in MAE is observed after 2-day aging, equally attributed to photobleaching and secondary organic aerosol ~~(SOA) formation, while the subsequent slight decrease during further aging to 7 days is dominated by SOA formation.~~formation. Although a negative correlation is observed between particle size and MAE, the reduction in MAE is mainly driven by the decline in the imaginary part (k) of BrC, with particle size playing a minor role. Combined with positive matrix factorization (PMF) analysis, the study reveals that oxygenated OA, characterized by higher O/C ratios but lower MAE, increases significantly with aging. In contrast, two hydrocarbon-like OA factors with lower O/C ratios and higher MAE, decrease over time. These results emphasize the importance of categorizing BrC based on its MAE and atmospheric behavior

in climate models.

1 Introduction

As a special class of organic aerosol (OA), brown carbon (BrC) exhibits a significant light absorption ability at near-UV and
30 shorter visible wavelengths with a strong wavelength dependence (Laskin et al., 2015). It accounts for approximately 19–40%
of the total absorption by carbonaceous particles (Feng et al., 2013; Lin et al., 2014), with a global radiative forcing ranging
from +0.03 to +0.57 W m^{-2} (Li et al., 2023a). BrC can also perturb the temperature structure of the atmosphere and then
influence cloud cover, known as semi-direct effects (Laskin et al., 2015; Yan et al., 2018). When deposited on snow and ice,
BrC can reduce surface albedo and cause early snow melting (Qian et al., 2015; Tuccella et al., 2021). Additionally, the strong
35 UV-absorption due to BrC can reduce the rate of atmospheric photochemical reactions, resulting in a 15%–30% decrease in
regional concentrations of OH radical and O_3 (Wang et al., 2022). However, current understanding of the BrC light absorptivity,
especially its evolution upon aging processes, remains limited, driving a significant uncertainty in the estimates of its climate
effects.

BrC originates from a variety of sources, including primary emissions from biomass burning, coal combustion~~,~~ and vehicular
40 emissions (Olson et al., 2015; Sun et al., 2017; Xie et al., 2017a; Park et al., 2018), as well as secondary processes such as
photochemical oxidation (Lambe et al., 2013; Xie et al., 2017b), aqueous-phase processes (Lin et al., 2015; Ye et al., 2019)
and nighttime oxidation (Jiang et al., 2019; Chen et al., 2023). Among these sources, biomass burning has long been recognized
as a dominant source (Saleh, 2020). When ~~OA~~considering BrC light absorption ~~from biomass is considered~~, the overall
regional or global radiative forcing ~~from~~of biomass burning aerosol can ~~change~~shift from negative to positive effects~~, reaching
45 up to +0.05 W m^{-2}~~ (Saleh et al., 2015).

Many laboratory and field studies have investigated the chemical and optical properties of BrC from biomass burning (Hems
et al., 2021). The ~~light absorptivity~~optical properties of freshly emitted BrC ~~has~~, such as the absorption Ångström exponent
(AAE) and mass absorption efficiency (MAE) or imaginary part (k), have been shown to ~~depend~~strongly depend on burning
conditions. ~~For instance, Huo et al. (2018) demonstrated that the mass absorption efficiency (MAE) decreased under high
50 moisture or stacking conditions. The absorption Ångström exponent (AAE) also varies,~~ with ~~the~~BrC from flaming biomass

burning ~~conditions,~~combustion exhibiting higher ~~during~~MAE and lower AAE than that from lower-temperature smoldering ~~than flaming stages (Martinsson~~combustion (Laskin et al., 2015; ~~Park et al.,~~Saleh, 2020). Utilizing the ratio of BC/OA as a proxy of the burning condition, several studies have established a quantitative relationship between the MAE and the burning conditions based on laboratory combustion experiments (Saleh et al., 2014; Xie et al., 2017a; Park et al., 2020). However, the relationship varies with different studies, and is suggested to be affected by the ~~types of~~ biomass types (Xie et al., 2017a; Park et al., 2020). So far, to what extent could the biomass types affect the BrC absorptivity is not clear and requires further study.

Upon aging processes, BrC absorptivity could decrease significantly due to the photobleaching of some chromophores, with a lifetime ranging from a few hours (Zhao et al., 2015; Browne et al., 2019) to a few days (Forrister et al., 2015; Sumlin et al., 2017). The photobleaching rate largely depends on ambient conditions, including concentrations of OH radical (Wang et al., 2014) and NO_x (Yang et al., 2022) as well as relative humidity and temperature (Klodt et al., 2023; Gao et al., 2024). The chemical characteristics of BrC also determine the extent of the photobleaching effect. For example, tar balls from biomass burning are found to be resistant to the photobleaching process (Saleh, 2020). Moreover, the light absorption of BrC can be enhanced ~~(i.e., photo-enhancement)~~ through the ~~nitration~~functionalization and polymerization of existing OA (Wong et al., 2019; Hems et al., 2020~~). For example, He et al. (2022) showed that the MAE increased with the NO_x/VOCs ratio due to~~) or the formation of ~~nitroaromatic~~new nitrogen-containing organic compounds~~.~~, e.g., nitroaromatics (He et al., 2022; Yang et al., 2022). The photobleaching and ~~photo~~ enhancement may occur concurrently, making the evolution of BrC absorptivity more complicated. Some studies reported continuously decrease ~~or increase~~ in MAE (~~Choudhary~~k (Liu et al., 202~~3~~1) while some show a slight increase first followed by a significant decrease (Cappa et al., 2020; Schnitzler et al., 2020~~, Fang et al., 2022~~). However, current studies mainly focus on the evolution of the overall BrC absorptivity~~,~~ and few have endeavored to distinguish the behaviors of different BrC components~~,~~ (Wong et al., 2019; Fleming et al., 2020), which may undergo totally different aging processes.

In this study, we characterized the optical, physical, and chemical properties of fresh and aged BrC emitted from biomass combustion. By analyzing the synchronous evolution of both chemical components and light absorption in the smoke, we explored the aging processes of different BrC components and their contributions to the overall light absorption at different aging levels. The study demonstrated significant discrepancies in the aging processes among different BrC components and

suggested the necessity to classify BrC based on its optical properties, especially its photobleaching rate, for its better representation in climate models.

2 Materials and methods

2.1 Experimental setup

80 Five types of biomass fuels were collected from major crop producing areas in China, including wheat straw (WS), rice straw (RS), corn straw (CS), soybean straw (SS) and apple branch (AB) (Table S1 and Fig. S1). The rice is mainly distributed in central and southern China, and others are mainly distributed in northern China. These biomass types could represent the majority of China's biofuels. The combustion experiments were conducted at the Institute of Earth Environment, Chinese Academy of Sciences (IEECAS) in Xi'an, China. Figure S2 illustrates the instrument configuration. Emissions were generated

85 by burning batches of ~10 g of dry biomass fuels (cut into pieces of 10–15 cm) on a combustion platform in a ~8 m^3 combustion chamber. After the flame was extinguished, the smoke was first mixed and allowed to stand in the combustion chamber, and was then diluted before being sampled by several online instruments. Details of the chamber and combustion facilities are provided in Tian et al. (2015).

A Potential Aerosol Mass-Oxidation Flow Reactor (PAM-OFR) (Aerodyne Research, LLC, Billerica, MA, USA) was

90 applied to simulate atmospheric aging processes. For each test, the fresh (F) aerosols were measured in the first 40 minutes and then the UV light of PAM-OFR was turned on for the next 40 minutes to measure the aged aerosols. Detailed information of the PAM-OFR is described by Cao et al. (2020). Briefly, inside the PAM-OFR, OH radicals were formed through a series of photochemical reactions of H$_2$O and O$_2$ under ~~the~~185 nm UV illumination ~~of UV light. Simulated~~. The simulated OH concentrations ~~could~~can thus be controlled via ~~tuning~~adjusting the UV light intensity ~~of UV light. Combined with~~. In this study,

95 two aging levels were simulated by applying two distinct UV intensities. For each aging level, the UV intensity was kept constant throughout the experiment by regulating the lamp voltage. Based on the residence time within the PAM-OFR (~~90s~~90 s) and ~~the~~an assumed average atmospheric OH concentration ~~in the atmosphere (~~of 1.5 × 10^6 molecules cm^{-3}~~)~~ (Mao et al., 2009), the equivalent atmospheric aging levels were estimated to be around 2-days (A-2) and 7-days (A-7) in this study, similar

to those reported by Li et al. (2020) and Guo et al. (2022). Table S1 also summarizes the conditions for all burning tests in this study. It is important to note that the experimental conditions do not perfectly represent the photochemical conditions of the atmosphere, and it emphasizes OH-driven oxidation under initially high-NO_x conditions which rapidly shift towards low-NO_x conditions (Cappa et al., 2020).

2.2 Gas analysis

The CO and CO_2 concentrations were monitored using a Fourier Transform Infrared (FTIR) gas analyzer (DX4015, Gasmet, Finland). Before each group of experiments, we cleaned the FTIR sample cell with nitrogen and performed background measurements. Gas concentrations were treated by FTIR standard procedures (Calcmet v12.15) using the linear relationship between absorbance and molecular number combined with the reference spectra. The modified combustion efficiency (MCE), defined as $\triangle CO_2/(\triangle CO_2+\triangle CO)$, was used to indicate the burning conditions during each fire test (Akagi et al., 2011; Wang et al., 2020b; Zhao et al., 2022). Here, the $\triangle CO$ and $\triangle CO_2$ represent the background-corrected CO and CO_2 values in the smoke. The MCE measured in this work ranged from 0.95 to 0.99 (Table S1). An MCE value greater than 0.9 is indicative of flaming combustion (Sinha et al., 2003; Akagi et al., 2011). ~~Actually, flaming and smoldering phases occur simultaneously during a fire (Akagi et al., 2011; Wang et al., 2020b).~~ The NO_x and SO_2 concentrations were monitored both before and after the PAM-OFR (Fig. S2) using NO_x analyzers (model 42i, Thermo Scientific Inc., USA) and SO_2 analyzers (model 43i, Thermo Scientific Inc., USA), respectively. The consumption rate of NO_x and SO_2 during the aging process could then be derived base on their concentrations measured after the PAM-OFR relative those before the PAM-OFR.

2.3 Aerosol characterization

The mass concentrations of non-refractory chemical components were measured by a Time-of-Flight Aerosol Chemical Speciation Monitor (ToF-ACSM; Aerodyne Research Inc., USA), including organics, nitrate (NO_3^-), sulfate (SO_4^{2-}), chloride (Cl^-~~),~~ and ammonium (NH_4^+). ~~Detailed descriptions~~A detailed description of this instrument ~~are provided~~can be found in ~~Decarlo~~Fröhlich et al. ~~(2006~~(2013) and Xu et al. (2017). Briefly, the aerosols were first dried with a diffusion dryer and then passed through a critical orifice into a narrow beam via an aerodynamic lens. The aerosols were successively vaporized by a

heated surface (~600 °C), ionized via electron ionization, and detected by a mass spectrometer detector. The collection efficiency (CE) value was 0.5 in this study. (Middlebrook et al., 2012). The calibrations were performed by dried monodispersed (300 nm) ammonium nitrate and ammonium sulfate particles. The relative ionization efficiencies (RIEs) of

125 3.93 and 0.82 were used for ammonium and sulfate and the default values of 1.1, 1.4, and 1.3 were used for nitrate, organics, and chloride, respectively (Jimenez et al., 2003; Canagaratna et al., 2007). The ToF-ACSM data were analyzed with the standard data analysis software (Tofware v3.3) within Igor Pro (v7.08; WaveMetrics, Inc., Oregon, USA). In addition, Positive matrix factorization (PMF) (Paatero and Tapper, 1994) was performed on the high-resolution mass spectral matrix of OA (Ulbrich et al., 2009; Zhang et al., 2011). Finally, three OA factors were identified by the PMF model, including two

130 hydrocarbon-like OA (HOA-1 and HOA-2) and one oxygenated OA (OOA).

To quantify the photochemical effect on aerosol chemical compositions, we further calculated the enhancement ratio (*ER*) of different species using BC as a proxy for primary emissions (Eq. 1):

$$ER = \frac{X_{aged}}{BC_{aged}} / \frac{X_{fresh}}{BC_{fresh}}, \tag{1}$$

where X represents a certain species, e.g., NO_3^-, SO_4^{2-}, OA, or OOA. BC was measured via a seven-wavelength

135 Aethalometer (AE33) as described in the following section. The *ER* >1 indicates net production of species X while the *ER* <1 indicates net loss. Bias could be introduced by the assumption that different species have the same wall-loss rate (Hennigan et al., 2011). In addition, BC measured by AE 33 could also be biased by applying a fixed MAE value when converting the optical absorption to the mass concentration, which instead varies with BC mixing state (Zanatta et al., 2018).

In addition, we also investigated the evolution of aerosol size distributions along with the aging process and its possible

140 influence on estimated BrC MAE. The particle number size distribution was obtained via a Differential Mobility Analyser (DMA, Model 3082, TSI Inc., USA) combined with a Condensation Particle Counter (CPC, Model 3788, TSI Inc., USA), focusing on particles within a size range of approximately 12–460 nm.

2.4 Optical measurement

The light absorption of aerosols was measured with a seven-wavelength Aethalometer (Model AE33, Magee Scientific,

145 Berkeley, CA, USA). The AE33 measures light transmitted through a filter on which particles are deposited and automatically

compensates for the loading effect and multiple scattering coefficients (*C*) in real time (Drinovec et al., 2015; Drinovec et al., 2017). In this study, a newer filter tape (M8060) with a recommended *C* value of 1.39 was used. A value of 7.77 m^2 g^{-1} ~~for BC MAE~~was used to convert measured absorption at 880 nm ~~was adopted~~by AE33 to ~~calculate~~ the mass concentration of BC (Drinovec et al., 2015). The AAE is an important parameter to characterize the spectral dependence of aerosol absorption, and was calculated via Eq. 2:

$$b_{abs}(\lambda) = K \times \lambda^{-AAE},\tag{2}$$

where b_{abs} (λ) is the absorption coefficient at the wavelength of λ in unit of M m^{-1}, and *K* is a constant. The absorption coefficients of seven wavelengths were used to fit the exponential function curve to obtain AAE. Assuming BC is the only light-absorbing component at 880 nm (Kirchstetter et al., 2004; Kirchstetter and Thatcher, 2012), the b_{abs} of BC and BrC at 370 nm was then calculated by Eq. 3-4:

$$b_{abs,BC}(\lambda) = b_{abs}(880\ nm) \times \left(\frac{\lambda}{880}\right)^{-AAE_{BC}},\tag{3}$$

$$b_{abs,BrC}(\lambda) = b_{abs}(\lambda) - b_{abs,BC}(\lambda),\tag{4}$$

$$MAE(\lambda) = \frac{b_{abs,BrC}(\lambda)}{OA},\tag{5}$$

Here, AAE_{BC} was assumed to be 1.1, which represents the likely range of AAE for BC externally and internally mixed with non-absorbing materials (Lack and Langridge, 2013; Li et al., 2022b; Tian et al., 2023). Uncertainties may arise from the assumption that BC is the only light-absorbing component at 880 nm. A recent study suggested that tar BrC can also exhibit significant absorption at 880 nm, with MAE ranging from 0.2 to 1.8 m^2 g^{-1} (Corbin et al., 2019). Furthermore, the use of a fixed AAE_{BC} introduces additional uncertainty, as a wide range of 0.8−1.4 has been reported in previous studies (Lack and Langridge, 2013). The MAE of BrC at different λ were further calculated based on the mass concentrations of OA (Eq. ~~5). The ER of BrC absorption is also estimated by Eq. 1, where X represents BrC absorption in either fresh or aged smoke.~~5).

To further quantify the contributions of different OA components to BrC absorption, a multiple linear regression (MLR) model was applied to obtain the MAE values for HOA-1, HOA-2~~,~~ and OOA as follows:

$$b_{abs,BrC} = m_1 * [HOA - 1] + m_2 * [HOA - 2] + m_3 * [OOA],\tag{6}$$

Here, m_1, m_2 and m_3 denote the MAE, in unit of m^2 g^{-1}. The light absorption and MAE in this study refer to the wavelength at

170   370 nm, unless otherwise noted. The *ER* of BrC absorption was also calculated using a similar equation as for chemical components, with X representing the absorption of BrC at 370 nm and the BC term substituted by absorption at 880 nm.

3 Results and discussion

3.1 Chemical compositions of fresh and aged smoke

The chemical components of fresh and aged smoke from different biomass burning are illustrated in Fig. 1a. For fresh smoke,

175   the mass fraction of OA is the highest (39%–63%). The relative importance of BC and Cl^- varies significantly with biomass types. For example, the median mass fractions of BC emitted by ~~AB~~apple branch and ~~SS~~soybean straw are relatively high, reaching 22% and 27% respectively, but are only around 7.8%–10% by other biomass types, which instead exhibit higher mass fractions of Cl^- (21%–34%) and NH_4^+ (10%–13%). Relatively high mass fraction of Cl^- (>20%) was also reported in the smoke from straw combustion (Ni et al., 2017; Ma et al., 2019). This difference may be related to local crop fertilization, which

180   significantly affects the element content of the straw~~.~~ (Huan-Cheng et al., 2005). Higher MCE may also cause more emission of Cl^- due to higher burning temperatures (Wang et al., 2020b). The mass fractions of SO_4^{2-} and NO_3^- are very low (<5%) except for ~~AB~~apple branch, consistent with other laboratory results (Li et al., 2016; Ma et al., 2019; Guo et al., 2022). Upon the aging process, significant changes were found for aerosols with secondary sources, including SO_4^{2-}, NO_3^- and OA. For SO_4^{2-}, the *ER* is around 1.1–2.3 at A-2 and further increases to 1.7–3.1 at A-7 (Table S2). The *ER* of NO_3^- at A-2 (1.5–2.9) is

185   higher than that of SO_4^{2-}, which could be explained by a faster NO_3^- production rate and is also consistent with the higher NO_x consumption rate compared to SO_2 (Fig. S3). The *ER* of NO_3^- at A-7 (1.6–2.6), however, is similar to or even lower than that at A-2, and hence is significantly lower than that of SO_4^{2-}. Similar trends of SO_4^{2-} and NO_3^- from A-2 to A-7 have also been reported in other studies (Guo et al., 2022), and are attributed to the replacement of NO_3^- by more acidic SO_4^{2-}. ~~This could also explain the low *ER* value of Cl^- (<1).~~Similarly, Cl^- depletion can also result from acid replacement by stronger acids such

190   as H_2SO_4 and HNO_3 (Wang et al., 2019) or reactions with organic acids (Laskin et al., 2012), leading to a low *ER* value of Cl^- (i.e., *ER* < 1). Moreover, the cycle between NO_x and their oxidative reservoir (NO_z), has a significant impact on the NO_2/NO_z ratio, and the photolysis of particulate nitrate (pNO_3) is proposed as a potentially important mechanism influencing the

partitioning between NO_x and NO_z (Ye et al., 2023). However, the photolysis rate constant of pNO_3 is highly variable and can be greatly affected by aerosol properties, including pNO_3 loading and particle size (Ye et al., 2017; Andersen et al., 2023). This may also help explain the observed differences in the *ER* of NO_3^- between A-2 and A-7.
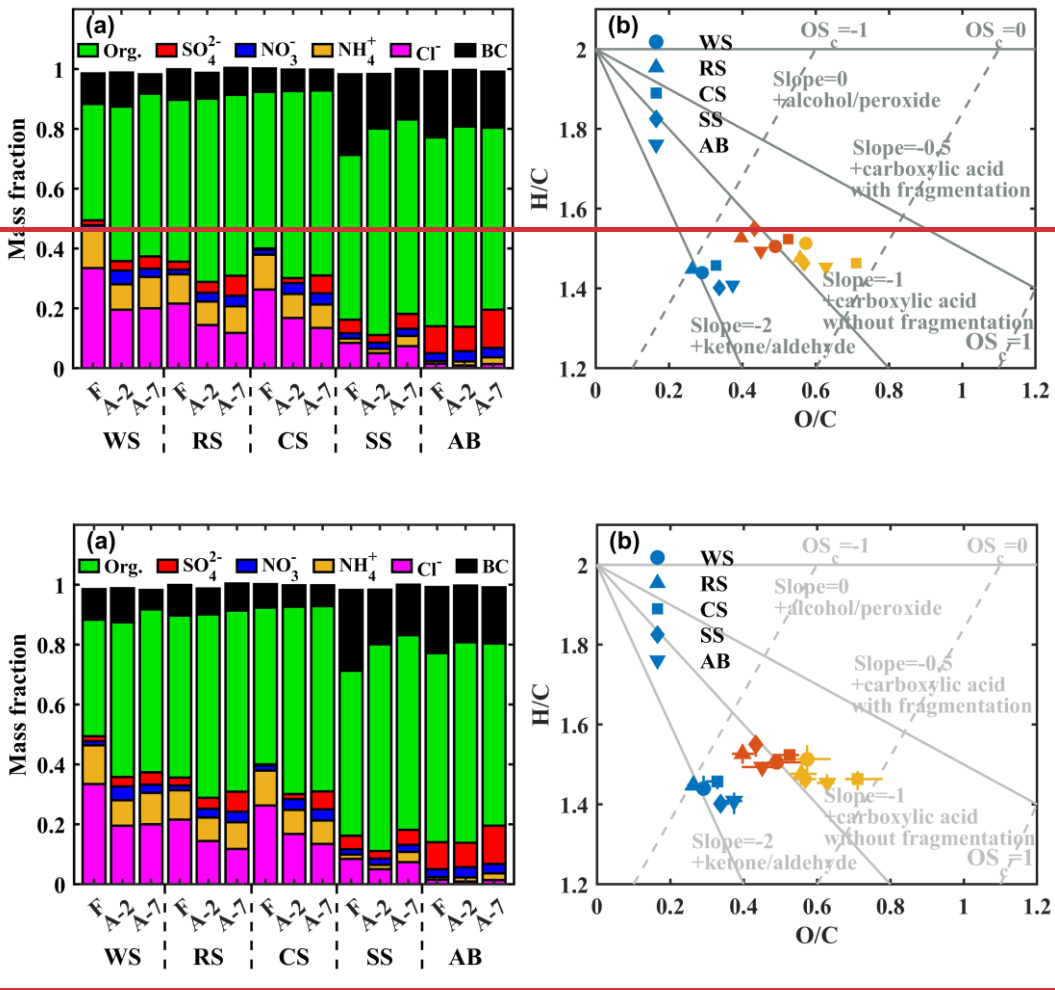
Figure 1. (a) The mass fractions of chemical components of different biomass smoke and (b) the Van Krevelen diagram of H/C versus O/C ratios for all OA. ~~Blue~~The solid markers and whiskers in (b) denote the median, 25th and 75th percentiles, respectively, and the blue, red and orange ~~dots~~ represent fresh (F), 2-days (A-2) and 7-days (A-7), respectively. The grey dotted lines represent the estimated carbon oxidation states ($OS_c \approx$ 2 O/C − H/C), and the grey solid lines represent the evolution of OA composition.

For OA, the *ER* increases from 1.3–1.6 at A-2 to 1.4–1.9 at A-7, showing continuous formation of secondary organic aerosols (SOA~-~). This could be verified by the stack diagram of the high-resolution mass spectra in Fig. S4, which demonstrates a

notable increase in signals at m/z 28 and 44 for all biomass types under the OH exposure, indicative of the formation of

oxygenated OA, such as organic acids (Aiken et al., 2008; Lambe et al., 2013). ~~As a result, the H/C and O/C ratios shift from~~

~~the region with a slope of −2 in fresh smoke to the region with a slope of −1 upon aging (Fig. 1b), implying an increase in~~

~~carboxyl group (−COOH) with a direct replacement of H. Compared with A-2, H/C is slightly reduced under A-7 due to the~~

~~hydrogen loss from the C=O bond formation (Lambe et al., 2013).~~ To further describe the implied changes in OA composition,

the H/C and O/C ratios for both fresh and aged smoke are distributed on the Van Krevelen diagram in Fig. 1b. The ratios are

estimated based on high-resolution fragments (i.e., m/z of 43 and 44) using calibration factors from Canagaratna et al. (2015),

which derived these factors from sampling standards, assuming that the elemental composition of the original species

corresponds to the averaged ion composition across the mass spectrum. The H/C and O/C values of fresh OA are 1.44 and

0.33, respectively, indicating a low carbon oxidation state ($OS_c \sim -1$). Compared to fresh OA, the O/C ratios progressively

increase to 0.45 for A-2 and 0.57 for A-7, accompanied by an OS_c approaching 0, which is attributed to the formation of

oxygenated OA. The H/C ratios also show an increase (1.52) for A-2 but slightly decrease for A-7 compared to A-2. The

evolution of H/C depends on the precursor, and in general it decreases with OH exposure due to the hydrogen loss from the

C=O bond formation (Lambe et al., 2013). However, Hennigan et al. (2011) also reported a slight increase in H/C ratios. Li et

al. (2023b) attributed the discrepancy to the abundance of $C_2H_3O^+$ in fresh smoke, where low $C_2H_3O^+$ levels lead to an increase

in m/z 43 during initial aging process.

3.2 OA classification based on PMF

~~−~~To further explore the evolution of different OA components, we classified total OA from both fresh and aged smoke into

~~three~~different categories based on the PMF model. We ran the model with the number of factors ranging from 2 to 7 and chose

three factors for the final results based on optimal fit and interpretability (Fig. 2). Factor 1, classified as HOA-1, has the lowest

O/C ratio (0.08) and shows strong correlations with ions at m/z 55 ($r^2 = 0.85$) and 57 ($r^2 = 0.90$), respectively. Many field

observations indicate that this factor is usually related to different combustion processes (Thamban et al., 2017; Rivellini et al.,

2020; Li et al., 2022a). Factor 2, classified as HOA-2, is also characterized by hydrocarbon fragments, especially at m/z of 41,

43, 55, 57, 67, 69~~,~~ and 71. It has moderate ratios of O/C (0.37) and H/C (1.2) compared to other factors. It also has a good

correlation with BC ($r^2 = 0.50$), ions at m/z 60 ($r^2 = 0.41$) and 73 ($r^2 = 0.68$), respectively (Table S3), which is also similar to the HOA resolved from ambient OA (Thamban et al., 2017; Li et al., 2017; Wang et al., 2020a). Factor 3 is dominated by ions at m/z 28 and 44 with the highest O/C ratio of 0.76. Moreover, it is well correlated with oxidized products or fragments, including SO_4^{2-} ($r^2 = 0.51$), NO_3^- ($r^2 = 0.58$), m/z 28 ($r^2 = 0.72$) and m/z 44 ($r^2 = 0.90$), and thus is classified as OOA.~~–~~

For fresh smoke, the OA is dominated by HOA-1 and HOA-2, while the contribution of OOA is still of significance (19%–40%, Fig. 2d). This is actually a significant feature distinguishing biomass sources from other sources~~, such as traffic exhaust (Thamban et al., 2017; Wu et al., 2019).~~ (Aiken et al., 2008). Biomass is naturally rich in oxygen-containing compounds, such as cellulose, hemicellulose and lignin. And those oxygen-containing structures partially break down and release oxygen-rich substances into the gas or aerosol phase during combustion. Incomplete combustion during ignition and the burnout stages can also produce oxidized OA with relatively high O/C ratios (Heringa et al., 2011; Avery et al., 2023). Previous studies have reported O/C ratios of 0.2–0.6 in fresh biomass burning smoke (Heringa et al., 2011; Fang et al., 2017; Ma et al., 2019; Li et al., 2023b), significantly higher than those from traffic exhaust (around 0.02–0.19) (Chirico et al., 2010; Dallmann et al., 2014; Collier et al., 2015). Along with OH exposure, the fractions of HOA-1 and HOA-2 decrease while OOA increases significantly, reaching 55%–70% at A-2 and 62%–80% at A-7, respectively. For HOA-1, the *ER* for all biomass types decreases from 0.88 at A-2 to 0.66 at A-7, respectively. The *ER* of HOA-2 is around 0.63 at A-2, but slightly increases to 0.71 at A-7. The *ER* of OOA of different biomass types reaches 2.6–3.7 at A-2, implying significant and fast yields of SOA. The *ER* of OOA continues to grow at A-7 but the growth rate slows down compared to A-2. Previous studies have also shown that the initial rapid increase of SOA and O/C in biomass burning aerosols slows down with aging time (~~>~~exceeds 2 day~~)~~s due to the depletion of precursors (Grieshop et al., 2009; Cappa et al., 2020; Li et al., 2024). It is worth mentioning that there exists a large variability in OA composition as well as its evolution upon aging among different biomass types. For instance, the *ER* of OOA in AB smoke is the smallest and the difference between A-2 and A-7 is minor, while the *ER* of OOA in ~~WS~~wheat straw smoke increased by nearly 63% from A-2 to A-7.

250
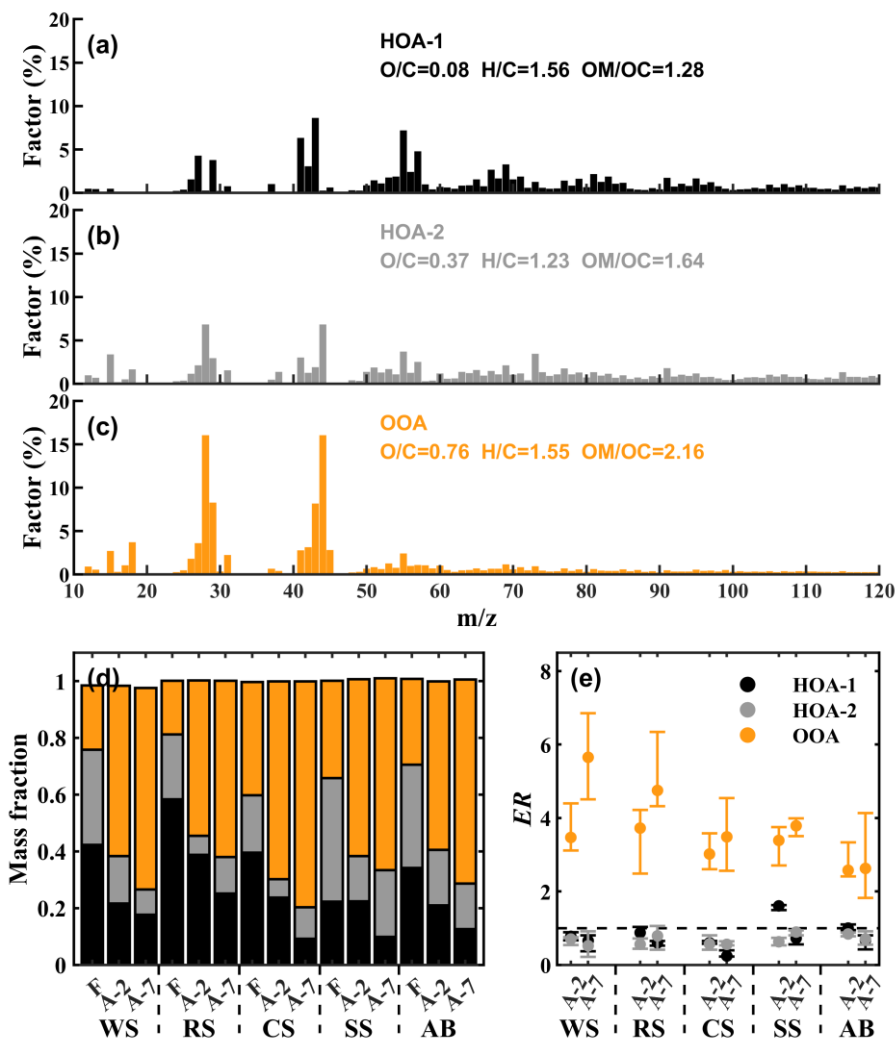
Figure 2. (a-c) High-resolution mass spectra of the three OA factors. (d) The median mass fractions and (e) the enhancement ratio (*ER*) of different OA factors at different aging levels. The solid circles and whiskers in (e) denote the median, 25th and 75th percentiles, respectively.

3.3 Evolution of particle size

255 The particle number size distribution of ~~different~~freshly emitted biomass smoke exhibits a unimodal lognormal distribution. After PAM aging, it exhibits a bimodal pattern, with an additional small-particle mode (around 20 nm) compared to fresh smoke, mainly resulting from nucleation. Here we only focus on the evolution of particles in accumulation mode. The

maximum peak diameter (D_m) and half-peak widths (σ) of Gaussian fits are shown in Fig. 3. The ~~WS~~wheat straw shows the largest D_m (239 nm) of freshly emitted biomass aerosols, followed by ~~CS~~corn straw (233 nm), ~~SS~~soybean straw (204 nm), ~~RS~~rice straw (178 nm) and ~~AB~~apple branch (162 nm). The D_m is within the range (50–500 nm) reported by Chen et al. (2019). Previous studies also show that the wheat smoke has a higher D_m in residue crops (Fang et al., 2017; Chen et al., 2019). Variations in D_m is related to both biomass types and combustion conditions (Park et al., 2013; Ma et al., 2019), such as fuel to air ratio, moisture content and density. ~~It~~Furthermore, it can be seen that ~~RS~~rice straw has the smallest σ (0.22), while ~~AB~~apple branch has the largest σ (0.28) and error bar (Fig. 3b), ~~implying relatively uniform morphology or density~~indicating that the particle number size distribution of ~~freshly emitted particles from RS compared to those from AB~~apple branch is the widest, while that of rice straw is the narrowest.
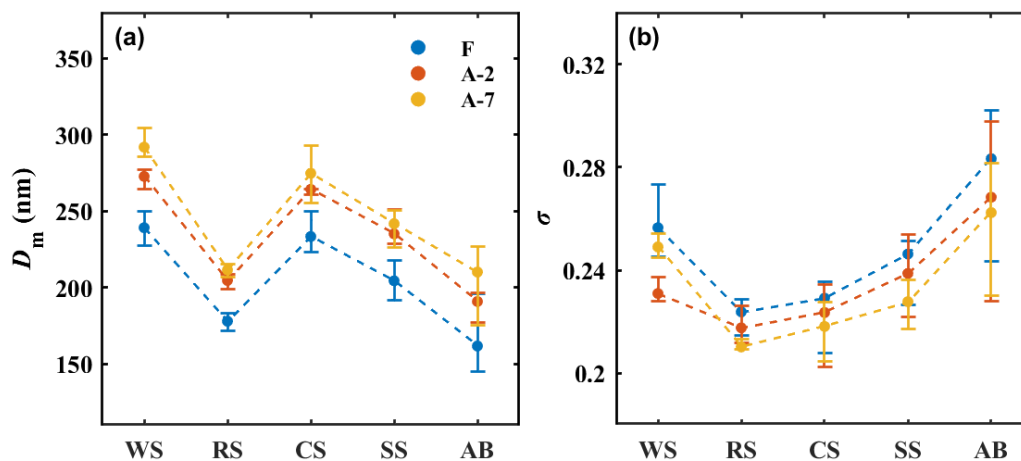
Figure 3. (a) The maximum peak diameter (D_m) and (b) half-peak widths (σ) from Gaussian fits for particle number size distribution. The solid circles and whiskers denote the median, 25th and 75th percentiles, respectively.

A significant increase in D_m is observed with increasing OH exposure, about 15% and 17% increase for A-2 and A-7, respectively. Similar change has also been reported in previous studies. For instance, Ma et al. (2019) reported a 1.1–1.4 times increase in particle size during 4-hour aging and Zhao et al. (2022) showed 1.2 times increase after 15-day photooxidation. The increase for 7-day is only slightly higher than that for 2-day, indicating a significant slowdown in particle growth. Many studies have also shown that D_m in biomass burning aerosols increases slowly after a rapid increase upon OH exposure (Fang

275 et al., 2017; Reyes et al., 2019). This could be explained, on one hand, by the limited availability of precursors. On the other hand, as particles grow, more mass is required to increase their diameter by one unit ~~particle size as the particle grows. This may also explain the observed decease~~. Consequently, smaller articles grow faster in ~~σ as particles shift~~diameter, leading to ~~larger size along with~~a narrower size distribution and a reduced σ upon aging (Fig. 3b).

3.4 Light absorption properties

280 A significant BrC contribution to the total light absorption in fresh smoke is observed but with a large variability across different biomass types (f_{BrC} = 29%–60%, Fig. 4). These values are in the middle range of the results in previous studies (~10%–90%) (Tian et al., 2019; Zhang et al., 2020; Fang et al., 2022). The presence of BrC makes the AAE of total aerosol significantly deviated from 1, with the highest value for ~~RS~~rice straw (2.3), followed by ~~CS~~corn straw (1.8), ~~AB~~apple branch (1.6), ~~WS~~wheat straw (1.5) and ~~SS~~soybean straw (1.4). These AAE values are also within the range of previous studies for biomass burning

285 aerosols (Laskin et al., 2015). Under OH exposure, the AAE decreases due to a reduction in BrC light absorption, with the *ER* of $b_{abs, BrC}$ around 0.51–0.85 and 0.63–0.90 in A-2 and A-7, respectively. The difference is statistically significant with $p < 0.05$, except for rice samples. The large decrease in BrC absorption at A-2 implies a significant effect of photobleaching. ~~The slight increase~~ associated with OH-driven oxidation in the PAM. No significant difference is observed in the *ER* of BrC absorption ~~at A-7 compared with that at~~between A-2 ~~on the one hand implies the effect of photo enhancement associated with the SOA~~

290 ~~formation,~~ and ~~on the other hand suggested~~A-7, indicating a limited photobleaching effect after 2-day aging. It has been reported that 20%–64% of BrC absorption remains even after a longer aging level (Sumlin et al., 2017; Browne et al., 2019; Hems et al., 2021), consistent with our results. Additionally, an exponential relationship between AAE and f_{BrC} is clearly observed (AAE = 0.97*exp (1.4*f_{BrC}), with 95% confidence intervals of 0.93–1.02 and 1.29–1.52 for the former and latter coefficients, respectively). Similar relationship has also been reported by Sun et al. (2021) for fresh household biomass burning

295 smoke, with AAE = 1.01*exp (1.8*f_{BrC}), which falls within the uncertainty range of our results. And our results further demonstrate that the relationship stands for both fresh and aged biomass burning emissions.
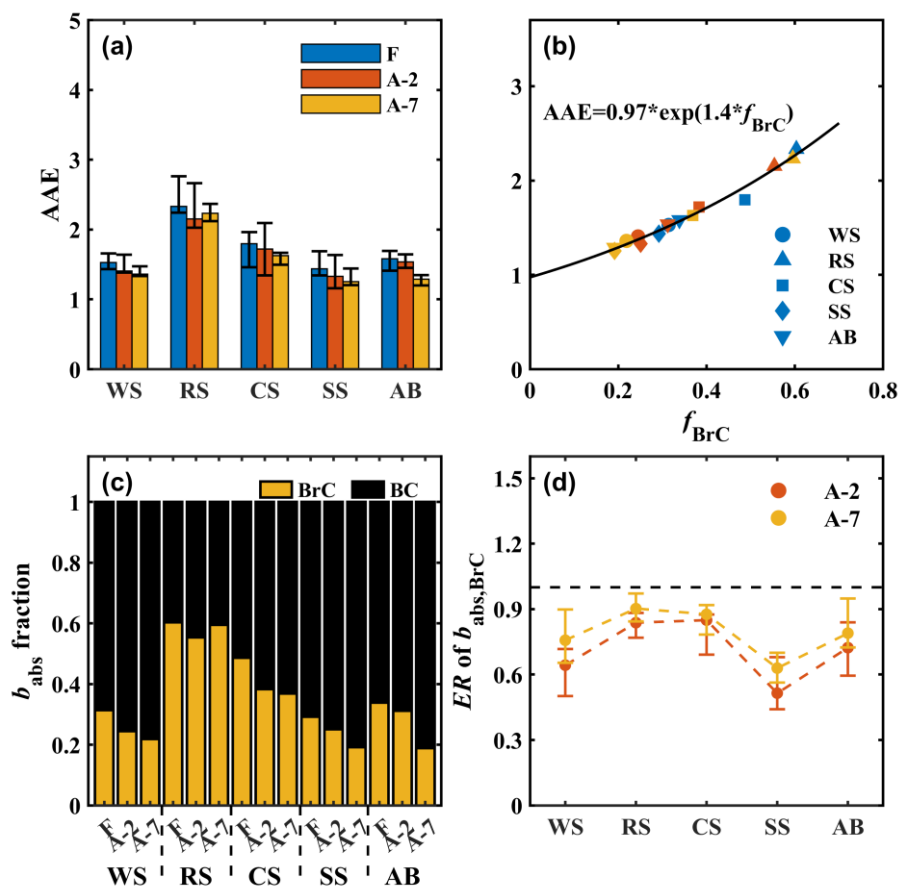
Figure 4. (a) AAE of total aerosol and (b) its relationship with BrC contribution to the total light absorption (f_{BrC}) at 370 nm; (c) relative contribution of BrC and BC to total light absorption at 370 nm; and (d) the enhancement ratio (*ER*) of BrC absorption.

300   In addition to the variation in BrC absorption, the MAE of fresh OA emitted from different biomass burning also exhibits a large range, with the highest value from ~~RS~~rice straw (5.7 m² g⁻¹), followed by ~~AB~~apple branch (3.9~~), SS~~ m² g⁻¹), soybean straw (3.7~~), CS~~ m² g⁻¹), corn straw (3.5~~),~~ m² g⁻¹) and ~~WS~~wheat straw (2.1 m² g⁻¹) (Fig. 5a). Upon OH exposure, ~~A~~a large decrease in the MAE is observed, reduced by 32%–64% and 37%–68% at A-2 and A-7, respectively, compared with fresh. The change in MAE is associated with the changes in both BrC absorption and OA mass concentrations. In other words, it is

305   due to the combined effect of ~~photo~~bleaching and the formation of SOA with weak absorption. ~~For OA at A-2~~Compared to fresh smoke, the ~~reduction~~$b_{abs, BrC}$ at A-2 is reduced by about 15%–49%, accounting for roughly half or more of the change in MAE ~~compared to the fresh smoke.~~ This suggests that the reduction in MAE at A-2 is dominated ~~comparably~~ by both ~~the~~

changes in $b_{abs, BrC}$ and OA mass. ~~Compared to~~Moreover, the ~~condition of A-2, the reduction in MAE is mainly driven by the increasing in SOA with weak absorption. This again suggests~~MAE of rice straw, corn straw and soybean straw at A-7 is similar to that in A-2, which may imply the resistance of BrC to photobleaching after the first few days of aging. Similarly, Zhao et al. (2022) also reported that 49% to 67% of the initial MAE of rice straw remained after equivalent 9 days of aging.

To further distinguish the light absorptivity of different OA components, we calculated the MAE of the three OA factors based the MLR method (Fig. 5b). There exists a significant difference in the MAE of the three OA factors, with the highest value (5.6 m² g⁻¹) for HOA-1, followed by HOA-2 (4.0 m² g⁻¹) and OOA (0.76 m² g⁻¹). The decrease in the MAE with the increase in O/C ratio is consistent with previous findings (Sumlin et al., 2017; Schnitzler et al., 2020; He et al., 2022). As discussed above, the evolutions of three OA factors are quite different during the aging process, their contribution to the light absorption thus varies significantly. For A-2 and A-7, the *ER* of $b_{abs, BrC}$ for HOA-1 are 0.85 and 0.60, respectively, and HOA-2 shows similar values of 0.69 and 0.79. Contrarily, OOA exhibits the highest *ER* of $b_{abs, BrC}$ (3.2 and 4.0, respectively). Consequently, the contribution from OOA absorption increases from 6% at fresh to 19% at A-2 and 26% at A-7, respectively, while the contribution from HOA-1 absorption decreases from 65% at fresh to 59% at A-2 and 43% at A-7, respectively, and that from HOA-2 remains similar (23%–30%) (Fig. S6). The significantly different behavior of the three OA factors combined with their distinct MAE values suggest the importance in climate models to classify OA into different groups based on their optical properties, which could be represented by the oxidation sate in this case.
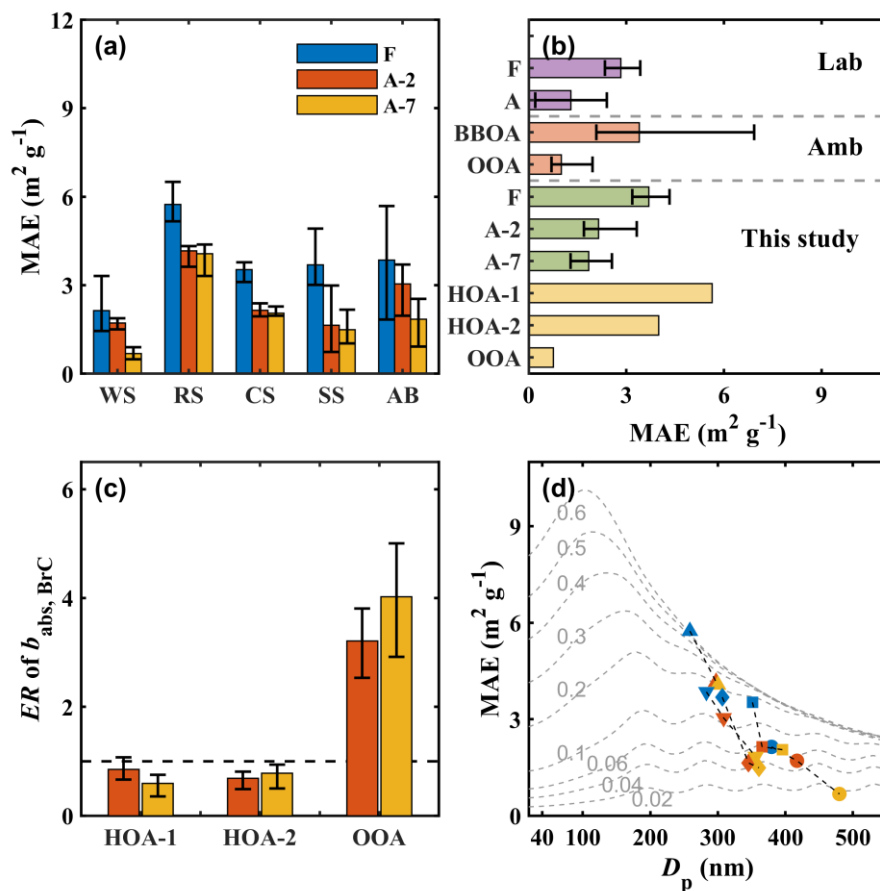
Figure 5. (a) MAE of BrC at 370 nm and (b) comparison of BrC MAE in this study with previous studies including both laboratory measurements and field observations (see details and corresponding references in Table S4 and S5); (c) the enhancement ratio (*ER*) of BrC absorption in different OA factors; (d) relationship of MAE at 370 nm with particle diameter (*D*$_p$), the blue, red and orange dots represent the peak sizes of the particle mass size distribution from fresh (F), 2-days (A-2) and 7-days (A-7), respectively. Note that the MAE of OC in some studies has been converted to the MAE of OA assuming OA/OC equal to 1.8; the MAE dependence on particle size in (d) is calculated using the Mie model for pure BrC (gray dashed lines).

Additionally, we found that the MAE of OA decreases with the increases of particle size (Fig. 5d). To explore the potential influence of particle size on the variation in BrC MAE, we conducted a theoretical calculation of the MAE for pure BrC particles as a function of D_p using Mie theory. Assuming that the BrC particles are spherical with as a density of 1.6 g cm^{-3}, the MAE for BrC particles at a specific diameter can be determined, given a particular refractive index. In this study, we adopt the real part (*n*) of the refractive index of pure BrC is 1.7 from Saleh et al. (2014) and the ~~imaginary part (*k*)~~ varies from 0.6 to

0.02. As shown in Fig. 5d, for a fixed particle diameter, the BrC MAE increases with k. The relationship between particle diameter and MAE is more complicated even with the refractive index remains constant. For small particles (<100 nm), the MAE generally increases with diameter (gray dashed lines). However, for large particles, the MAE decreases with diameter given a larger k value but exhibits weak fluctuations and no obvious trends when k is small, which is consistent with previous

340   studies (Hems et al., 2021). The median diameters of BrC particles in both fresh and aged biomass burning plume detected in this study are in the region where MAE either decreases with diameter or shows minimal dependence on diameter (Fig. 5d). Therefore, the large reduction in MAE is mainly driven by changes in k, specifically, lower k values at larger D_{p}. As discussed earlier, upon OH exposure, there is a significant increase in particle size with new components formation (Fig. 3). The latter is dominated by more contribution from OOA with high O/C (Fig. S5b), which has much lower MAE or k compared to the other

345   two OA factors.

For better comparison, Fig. 5b also summarizes MAE values for biomass burning OA reported from both laboratory measurements and field observations. The MAE of fresh BrC either measured in the laboratory or derived from ambient observations shows a large variability but has a similar range as with our results. This large variability is primarily attributed to differences in biomass types and burning conditions. As mentioned above, the MAE or k of biomass burning OA could be

350   expressed as a function of BC/OA, accounting for the influence of burning conditions (Saleh et al., 2014; Pokhrel et al., 2016). Here, we found similar relationship with a linear regression slope of 8.0 (Fig. S5a~~), which is within the range (~ 0.63~22) of the slope reported in previous studies ()~~. Xie et al~~.,~~. (2017a~~;~~) and Park et al~~.,~~. (2020~~).~~) also reported a slope of approximately 0.63 and 28, respectively, for biomass burning smoke. The large differences in the slope may be due to variations in the biomass type and combustion conditions. The MAE for aged OA is still very limited in laboratory measurements, with a value around

355   1.4~~3~~ m^2 g^{-1} that largely depends on the simulated aging levels. This is also consistent with our results, 2.1 and 1.8 m^2 g^{-1} for OA at A-2 and A-7, respectively. The MAE of SOA derived from ambient observations is slight lower. This is because SOA from ambient studies includes precursors from sources other than biomass burning. It has been shown that SOA from biogenic sources is less light-absorbing compared to that from anthropogenic sources, including biomass burning (Du et al., 2014).

4 Conclusions

The optical, physical and chemical properties of the biomass burning smoke upon aging were monitored simultaneously to better understand the evolution of biomass burning aerosol, especially BrC, and its driving factors. Upon OH exposure, the fraction of secondary components increases significantly, and the increase in OA is associated with the rising value of O/C~,~ ~~mainly for the carboxyl group.~~. However, the behavior of the secondary components differs significantly at different aging

370 levels. The ER of NO_3^- at A-2 is similar to or lower than A-7, probably due to the replacement of NO_3^- by more acidic SO_4^{2-}, or the photolysis of particulate nitrate. The ER of OA at A-2 and A-7 are also very similar, but due to limited availability of precursors. The particle number size distribution of fresh biomass smoke exhibits a unimodal lognormal distribution. Particle growth is mainly dominated by the formation of SOA and thus shows a similar trend as OA upon aging.

The optical properties of the biomass burning obtained in this study are in general within the wide range reported in previous
375 studies, including the relationship between the AAE of total aerosol and the fraction of BrC absorption, the dependence of BrC MAE on the BC/OA ratio, and the presence of some BrC resistant to photobleaching.. The large variation in the quantified relationship, however, emphasizes the significant influence from the biomass types and warrants more studies. The extent of the photobleaching as well as the formation of SOA with weak absorptivity together determine the evolution of BrC MAE at different aging levels. There exists a large decrease in BrC MAE from fresh smoke to A-2, contributed comparably by both
380 the photobleaching in BrC absorption and the increase in SOA. Only a slight decrease in BrC MAE is found from A-2 to A-7 and is mainly caused by the small increase in SOA where the photobleaching effect is very limited. We also observed a negative correlation between the MAE and the particle size. However, based on the Mie theory calculation, we found that the change in MAE is mainly driven by the change in the imaginary part (k) of OA instead of the particle size, implying lower k value at larger particle size. This is consistent with the formation of SOA with lower MAE (i.e. k) upon aging, which dominates the
385 particle growth. Therefore, it is important to distinguish the behavior of different OA components and their contribution to BrC absorption.

The study further classified the OA into three factors based on the PMF model, among which, HOA-1 and HOA-2 are more related to fresh smoke while OOA is associated with secondary formation with higher O/C value. The MAE of different OA factors also differ from each other, decreasing as the O/C value increases. The behavior of different OA factors upon aging
390 also shows distinct patterns, with a significant decrease in HOA-1 and HOA-2 but an increase in OOA. For A-2 and A-7, the ER of $b_{abs, BrC}$ for HOA-1 are 0.85 and 0.60, respectively, and HOA-2 shows similar values of 0.69 and 0.79. Contrarily, OOA exhibits the highest ER of $b_{abs, BrC}$ (3.2 and 4.0, respectively). Our results thus demonstrate the necessity of classifying OA into different categories based on their distinct MAE and behavior upon aging. Future studies should focus on the evolution of

different OA groups rather than the whole OA, which could be classified by their O/C value, solubility, etc., to develop more appropriate BrC parameterization in model studies for better assessing its climate effects.

Code and data availability. The ~~code and~~codes used to curate and analyze the datasets and produce the figures and results of the study are available from the corresponding author upon request. The data supporting the conclusions of this paper are available ~~upon request Qiaoqiao Wang (qwang@jnu.edu.cn) and Qiyuan Wang (wangqy@ieecas.cn).~~from https://doi.org/10.5281/zenodo.15493841.

Author contributions. QQW, QYW, NM, JT and YQZ conceptualized and designed the study. NM, QYW and YFW provided instrumentation and experimental materials. ZY, GX, MG, XXZ, YZ and WKR performed the laboratory measurements. ZY completed the formal data analysis and prepared the original manuscript draft with the help of QQW, NM, QYW, JCT, JH, JT, NY, YQZ, JJC, HS and YFC. All the authors reviewed, edited, and contributed to the scientific discussion in the manuscript.

Competing interests. The authors declare that they have no conflict of interest. Some authors are members of the editorial board of journal X.

Acknowledgements. We gratefully acknowledge the Institute of Earth Environment of Chinese Academy of Sciences (IEECAS) for the provision of the experimental site, equipment and technology. The authors gratefully thank the people at all sites for sample collections and all of the individuals and groups that participated in this project.

Financial support. The work was supported by the special fund of National Natural Science Foundation of China (grant nos. 42377093 and 42375072), Guangdong Basic and Applied Basic Research Foundation (grant no. 2024B1515040026), the National R&D Program of China (grant no. 2024YFC3712900), the National Key R&D Program of China (grant no. 2022YFF0802501), the "Western Light"–Key Laboratory Cooperative Research Cross-Team Project of Chinese Academy of Sciences (grant no. xbzg-zdsys-202219), the Guangdong Innovative and Entrepreneurial Research Team Program (Research Team on Atmospheric Environmental Roles and Effects of Carbonaceous Species: grant no. 2016ZT06N263), and Special Fund Project for Science and Technology Innovation Strategy of Guangdong Province (grant no. 2019B121205004).

References

Aiken, A. C., DeCarlo, P. F., Kroll, J. H., Worsnop, D. R., Huffman, J. A., Docherty, K. S., Ulbrich, I. M., Mohr, C., Kimmel, J. R., Sueper, D., Sun, Y., Zhang, Q., Trimborn, A., Northway, M., Ziemann, P. J., Canagaratna, M. R., Onasch, T. B., Alfarra, M. R., Prevot, A. S. H., Dommen, J., Duplissy, J., Metzger, A., Baltensperger, U., and Jimenez, J. L.: O/C and OM/OC Ratios of Primary, Secondary, and Ambient Organic Aerosols with High-Resolution Time-of-Flight Aerosol Mass Spectrometry, Environ. Sci. Technol., 42, 4478-4485, https://doi.org/10.1021/es703009q, 2008.

Akagi, S. K., Yokelson, R. J., Wiedinmyer, C., Alvarado, M. J., Reid, J. S., Karl, T., Crounse, J. D., and Wennberg, P. O.: Emission factors for open and domestic biomass burning for use in atmospheric models, Atmos. Chem. Phys., 11, 4039-

4072, https://doi.org/10.5194/acp-11-4039-2011, 2011.

Andersen, S. T., Carpenter, L. J., Reed, C., Lee, J. D., Chance, R., Sherwen, T., Vaughan, A. R., Stewart, J., Edwards, P. M., Bloss, W. J., Sommariva, R., Crilley, L. R., Nott, G. J., Neves, L., Read, K., Heard, D. E., Seakins, P. W., Whalley, L. K., Boustead, G. A., Fleming, L. T., Stone, D., and Fomba, K. W.: Extensive field evidence for the release of HONO from the photolysis of nitrate aerosols, Sci. Adv., 9, eadd6266, https://doi.org/10.1126/sciadv.add6266, 2023.

Avery, A. M., Fawaz, M., Williams, L. R., Bond, T., and Onasch, T. B.: Chemically distinct particle-phase emissions from highly controlled pyrolysis of three wood types, Atmos. Chem. Phys., 23, 8837-8854, https://doi.org/10.5194/acp-23-8837-2023, 2023.

Browne, E. C., Zhang, X., Franklin, J. P., Ridley, K. J., Kirchstetter, T. W., Wilson, K. R., Cappa, C. D., and Kroll, J. H.: Effect of heterogeneous oxidative aging on light absorption by biomass burning organic aerosol, Aerosol Sci. Technol., 53, 663-674, https://doi.org/10.1080/02786826.2019.1599321, 2019.

Canagaratna, M. R., Jimenez, J. L., Kroll, J. H., Chen, Q., Kessler, S. H., Massoli, P., Hildebrandt Ruiz, L., Fortner, E., Williams, L. R., Wilson, K. R., Surratt, J. D., Donahue, N. M., Jayne, J. T., and Worsnop, D. R.: Elemental ratio measurements of organic compounds using aerosol mass spectrometry: characterization, improved calibration, and implications, Atmos. Chem. Phys., 15, 253-272, https://doi.org/10.5194/acp-15-253-2015, 2015.

Canagaratna, M. R., Jayne, J. T., Jimenez, J. L., Allan, J. D., Alfarra, M. R., Zhang, Q., Onasch, T. B., Drewnick, F., Coe, H., Middlebrook, A., Delia, A., Williams, L. R., Trimborn, A. M., Northway, M. J., DeCarlo, P. F., Kolb, C. E., Davidovits, P., and Worsnop, D. R.: Chemical and microphysical characterization of ambient aerosols with the aerodyne aerosol mass spectrometer, Mass Spectrometry Reviews,Spectrom. Rev., 26, 185-222, https://doi.org/10.1002/mas.20115, 2007.

Cao, J., Wang, Q., Li, L., Zhang, Y., Tian, J., Chen, L. W. A., Ho, S. S. H., Wang, X., Chow, J. C., and Watson, J. G.: Evaluation of the Oxidation Flow Reactor for particulate matter emission limit certification, Atmos. Environ., 224, 117086, https://doi.org/10.1016/j.atmosenv.2019.117086, 2020.

Cappa, C. D., Lim, C. Y., Hagan, D. H., Coggon, M., Koss, A., Sekimoto, K., de Gouw, J., Onasch, T. B., Warneke, C., and Kroll, J. H.: Biomass-burning-derived particles from a wide variety of fuels – Part 2: Effects of photochemical aging on particle optical and chemical properties, Atmos. Chem. Phys., 20, 8511-8532, https://doi.org/10.5194/acp-20-8511-2020, 2020.

Chen, K., Mayorga, R., Hamilton, C., Bahreini, R., Zhang, H., and Lin, Y.-H.: Contribution of Carbonyl Chromophores in Secondary Brown Carbon from Nighttime Oxidation of Unsaturated Heterocyclic Volatile Organic Compounds, Environ. Sci. Technol., 57, 20085-20096, https://doi.org/10.1021/acs.est.3c08872, 2023.

Chen, L., Li, Q., Wu, D., Sun, H., Wei, Y., Ding, X., Chen, H., Cheng, T., and Chen, J.: Size distribution and chemical composition of primary particles emitted during open biomass burning processes: Impacts on cloud condensation nuclei activation, Sci. Total Environ., 674, 179-188, https://doi.org/10.1016/j.scitotenv.2019.03.419, 2019.

Choudhary, V., RosonChirico, R., DeCarlo, P. F., , M. L., Guo, X., Gautam,Heringa, M. F., Tritscher, T., Richter, R., Prévôt, A. S. H., Dommen, J., Weingartner, E., Wehrle, G., Gysel, M., Laborde, M., and Baltensperger, U.: Impact of aftertreatment devices on primary emissions and secondary organic aerosol formation potential from in-use diesel vehicles: results from smog chamber experiments, Atmos. Chem. Phys., 10, 11545-11563, https://doi.org/10.5194/acp-10-11545-2010, 2010.

Collier, S., Shan, Z., Toshihiro T., Gupta, T., and Zhao, R.: Aqueous phase photochemical oxidation of water soluble brown

carbon aerosols arising from solid biomass fuel burning, Environ. Sci.: Atmos., 3, 816 829, https://doi.org/10.1039/D2EA00151A, 2023.

DeCarlo, P. F., Kimmel, J. R., Trimborn, A., Northway, M. J., Jayne, J. T., Aiken, A. C., Gonin, M., Fuhrer, K., Sara, F., James, B., Mang, Z., Michael, K., Christopher, C., Timothy, B., and and Zhang, Q.: Organic PM Emissions from Vehicles: Composition, O/C Ratio, and Dependence on PM Concentration, Aerosol Sci. Technol., Horvath 49, 86-97, https://doi.org/10.1080/02786826.2014.1003364, 2015.

Corbin, J. C., Czech, H., Massabò, D., de Mongeot, F. B., Jakobi, G., Liu, F., Lobo, P., Mennucci, C., Mensah, A. A., Orasche, J., Pieber, S. M., Prévôt, A. S. H., Stengel, B., Tay, L. L., Zanatta, M., Zimmermann, R., El Haddad, I., and Gysel, M.: Infrared-absorbing carbonaceous tar can dominate light absorption by marine-engine exhaust, npj Clim. Atmos. Sci., 2, 12, https://doi.org/10.1038/s41612-019-0069-5, 2019.

Dallmann, T. R., Onasch, T. B., Kirchstetter, T., Docherty, K. S. W., Worton, D. R., Fortner, E. C., Herndon, S. C., Wood, E. C., Franklin, J. P., Worsnop, D. R., and Jimenez, J. L.: Field deployable, high resolution, time R., Goldstein, A. H., and Harley, R. A.: Characterization of flight particulate matter emissions from on-road gasoline and diesel vehicles using a soot particle aerosol mass spectrometer, Analytical chemistry, 78, 8281 8289 Atmos. Chem. Phys., 14, 7585-7599, https://doi.org/10.1021/ac061249n, 2006 5194/acp-14-7585-2014, 2014.

Drinovec, L., Močnik, G., Zotter, P., Prévôt, A. S. H., Ruckstuhl, C., Coz, E., Rupakheti, M., Sciare, J., Müller, T., Wiedensohler, A., and Hansen, A. D. A.: The "dual-spot" Aethalometer: an improved measurement of aerosol black carbon with real-time loading compensation, Atmos. Meas. Tech., 8, 1965-1979, https://doi.org/10.5194/amt-8-1965-2015, 2015.

Drinovec, L., Gregorič, A., Zotter, P., Wolf, R., Bruns, E. A., Prévôt, A. S. H., Petit, J. E., Favez, O., Sciare, J., Arnold, I. J., Chakrabarty, R. K., Moosmüller, H., Filep, A., and Močnik, G.: The filter-loading effect by ambient aerosols in filter absorption photometers depends on the coating of the sampled particles, Atmos. Meas. Tech., 10, 1043-1059, https://doi.org/10.5194/amt-10-1043-2017, 2017.

Du, Z., He, K., Cheng, Y., Duan, F., Ma, Y., Liu, J., Zhang, X., Zheng, M., and Weber, R.: A yearlong study of water-soluble organic carbon in Beijing II: Light absorption properties, Atmos. Environ., 89, 235-241, https://doi.org/10.1016/j.atmosenv.2014.02.022, 2014.

Fang, Z., Deng, W., Wang, X., He, Q., Zhang, Y., Hu, W., Song, W., Zhu, M., Lowther, S., Wang, Z., Fu, X., Hu, Q., Bi, X., George, C., and Rudich, Y.: Evolution of light absorption properties during photochemical aging of straw open burning aerosols, Sci. Total Environ., 838, 156431, https://doi.org/10.1016/j.scitotenv.2022.156431, 2022.

Fang, Z., Deng, W., Zhang, Y., Ding, X., Tang, M., Liu, T., Hu, Q., Zhu, M., Wang, Z., Yang, W., Huang, Z., Song, W., Bi, X., Chen, J., Sun, Y., George, C., and Wang, X.: Open burning of rice, corn and wheat straws: primary emissions, photochemical aging, and secondary organic aerosol formation, Atmos. Chem. Phys., 17, 14821-14839, https://doi.org/10.5194/acp-17-14821-2017, 2017.

Feng, Y., Ramanathan, V., and Kotamarthi, V. R.: Brown carbon: a significant atmospheric absorber of solar radiation?, Atmos. Chem. Phys., 13, 8607-8621, https://doi.org/10.5194/acp-13-8607-2013, 2013.

Fleming, L. T., Lin, P., Roberts, J. M., Selimovic, V., Yokelson, R., Laskin, J., Laskin, A., and Nizkorodov, S. A.: Molecular composition and photochemical lifetimes of brown carbon chromophores in biomass burning organic aerosol, Atmos. Chem. Phys., 20, 1105-1129, https://doi.org/10.5194/acp-20-1105-2020, 2020.

Forrister, H., Liu, J., Scheuer, E., Dibb, J., Ziemba, L., Thornhill, K. L., Anderson, B., Diskin, G., Perring, A. E., Schwarz, J. P., Campuzano-Jost, P., Day, D. A., Palm, B. B., Jimenez, J. L., Nenes, A., and Weber, R. J.: Evolution of brown carbon in wildfire plumes, Geophys. Res. Lett., 42, 4623-4630, https://doi.org/10.1002/2015GL063897, 2015.

Fröhlich, R., Cubison, M. J., Slowik, J. G., Bukowiecki, N., Prévôt, A. S. H., Baltensperger, U., Schneider, J., Kimmel, J. R., Gonin, M., Rohner, U., Worsnop, D. R., and Jayne, J. T.: The ToF-ACSM: a portable aerosol chemical speciation monitor with TOFMS detection, Atmos. Meas. Tech., 6, 3225-3241, https://doi.org/10.5194/amt-6-3225-2013, 2013.

Gao, P., Deng, R., Jia, S., Li, Y., Wang, X., and Xing, Q.: Effects of combustion temperature on the optical properties of brown carbon from biomass burning, J. Environ. Sci., 137, 302-309, https://doi.org/10.1016/j.jes.2022.12.026, 2024.

Grieshop, A. P., Logue, J. M., Donahue, N. M., and Robinson, A. L.: Laboratory investigation of photochemical oxidation of organic aerosol from wood fires 1: measurement and simulation of organic aerosol evolution, Atmos. Chem. Phys., 9, 1263-1277, https://doi.org/10.5194/acp-9-1263-2009, 2009.

Guo, X., Wang, X., Dai, W., Ho, K. F., Liu, S., Wang, Q., Shen, M., Liu, Y., Zhang, Y., Cao, Y., Qi, W., Li, L., Li, L., and Li, J.: Effects of atmospheric aging processes on carbonaceous species and water-soluble inorganic ions in biomass burning aerosols, Atmos. Environ., 288, 119322, https://doi.org/10.1016/j.atmosenv.2022.119322, 2022.

He, Q., Li, C., Siemens, K., Morales, A. C., Hettiyadura, A. P. S., Laskin, A., and Rudich, Y.: Optical Properties of Secondary Organic Aerosol Produced by Photooxidation of Naphthalene under NOx Condition, Environ. Sci. Technol., 56, 4816-4827, https://doi.org/10.1021/acs.est.1c07328, 2022.

Hems, R. F., Schnitzler, E. G., Liu-Kang, C., Cappa, C. D., and Abbatt, J. P. D.: Aging of Atmospheric Brown Carbon Aerosol, ACS Earth and Space Chem., 5, 722-748, https://doi.org/10.1021/acsearthspacechem.0c00346, 2021.

Hems, R. F., Schnitzler, E. G., Bastawrous, M., Soong, R., Simpson, A. J., and Abbatt, J. P. D.: Aqueous Photoreactions of Wood Smoke Brown Carbon, ACS Earth and Space Chem., 4, 1149-1160, https://doi.org/10.1021/acsearthspacechem.0c00117, 2020.

Hennigan, C. J., Miracolo, M. A., Engelhart, G. J., May, A. A., Presto, A. A., Lee, T., Sullivan, A. P., McMeeking, G. R., Coe, H., Wold, C. E., Hao, W. M., Gilman, J. B., Kuster, W. C., de Gouw, J., Schichtel, B. A., Collett Jr, J. L., Kreidenweis, S. M., and Robinson, A. L.: Chemical and physical transformations of organic aerosol from the photo-oxidation of open biomass burning emissions in an environmental chamber, Atmos. Chem. Phys., 11, 7669-7686, https://doi.org/10.5194/acp-11-7669-2011, 2011.

Huo, Y., LiHeringa, M., Jiang, M. F., DeCarlo, P. F., Chirico, R., Tritscher, T., Dommen, J., Weingartner, E., Richter, R., Wehrle, G., Prévôt, A. S. H., and Qi, W.: Light absorption propertiesBaltensperger, U.: Investigations of HULIS in primary and secondary particulate matter produced by crop strawof different wood combustion under different moisture contents and stacking modesappliances with a high-resolution time-of-flight aerosol mass spectrometer, Atmos. Environ., 191, 490-499Chem. Phys., 11, 5945-5957, https://doi.org/10.1016/j.atmosenv.2018.08.038, 20185194/acp-11-5945-2011, 2011.

Huan-cheng, P., Jin-song, Y., and Xiao-hong, X. I. E.: Effects of nitrogen fertilization on growth and vivo Cl- and Na+ accumulation of winter wheat under NaCl stress, J. Plant Nutr. Fert., 11, 654-658, https://doi.org/10.11674/zwyf.2005.0514, 2005.

Jiang, H., Frie, A. L., Lavi, A., Chen, J. Y., Zhang, H., Bahreini, R., and Lin, Y.-H.: Brown Carbon Formation from Nighttime Chemistry of Unsaturated Heterocyclic Volatile Organic Compounds, Environ. Sci. Technol. Lett., 6, 184-190,

https://doi.org/10.1021/acs.estlett.9b00017, 2019.

Jimenez, J. L., Jayne, J. T., Shi, Q., Kolb, C. E., Worsnop, D. R., Yourshaw, I., Seinfeld, J. H., Flagan, R. C., Zhang, X., Smith, K. A., Morris, J. W., and Davidovits, P.: Ambient aerosol sampling using the Aerodyne Aerosol Mass Spectrometer, J. Geophys. Res. Atmos., 108, https://doi.org/10.1029/2001JD001213, 2003.

540 Kirchstetter, T. W. and Thatcher, T. L.: Contribution of organic carbon to wood smoke particulate matter absorption of solar radiation, Atmos. Chem. Phys., 12, 6067-6072, https://doi.org/10.5194/acp-12-6067-2012, 2012.

Kirchstetter, T. W., Novakov, T., and Hobbs, P. V.: Evidence that the spectral dependence of light absorption by aerosols is affected by organic carbon, J. Geophys. Res. Atmos., 109, https://doi.org/10.1029/2004JD004999, 2004.

Klodt, A. L., Aiona, P. K., MacMillan, A. C., Ji Lee, H., Zhang, X., Helgestad, T., Novak, G. A., Lin, P., Laskin, J., Laskin, A.,
545 Bertram, T. H., Cappa, C. D., and Nizkorodov, S. A.: Effect of relative humidity, NOx, and ammonia on the physical properties of naphthalene secondary organic aerosols, Environ. Sci.: Atmos., 3, 991-1007, https://doi.org/10.1039/D3EA00033H, 2023.

Lack, D. A. and Langridge, J. M.: On the attribution of black and brown carbon light absorption using the Ångström exponent, Atmos. Chem. Phys., 13, 10535-10543, https://doi.org/10.5194/acp-13-10535-2013, 2013.

550 Lambe, A. T., Cappa, C. D., Massoli, P., Onasch, T. B., Forestieri, S. D., Martin, A. T., Cummings, M. J., Croasdale, D. R., Brune, W. H., Worsnop, D. R., and Davidovits, P.: Relationship between Oxidation Level and Optical Properties of Secondary Organic Aerosol, Environ. Sci. Technol., 47, 6349-6357, https://doi.org/10.1021/es401043j, 2013.

Laskin, A., Laskin, J., and Nizkorodov, S. A.: Chemistry of Atmospheric Brown Carbon, Chem. Rev., 115, 4335-4382, https://doi.org/10.1021/cr5006167, 2015.

555 Laskin, A., Moffet, R. C., Gilles, M. K., Fast, J. D., Zaveri, R. A., Wang, B., Nigge, P., and Shutthanandan, J.: Tropospheric chemistry of internally mixed sea salt and organic particles: Surprising reactivity of NaCl with weak organic acids, J. Geophys. Res. Atmos., 117, https://doi.org/10.1029/2012JD017743, 2012.

Li, C., Hu, Y., Chen, J., Ma, Z., Ye, X., Yang, X., Wang, L., Wang, X., and Mellouki, A.: Physiochemical properties of carbonaceous aerosol from agricultural residue burning: Density, volatility, and hygroscopicity, Atmos. Environ., 140, 94-
560 105, https://doi.org/10.1016/j.atmosenv.2016.05.052, 2016.

Li, H., Zhang, Q., Zhang, Q., Chen, C., Wang, L., Wei, Z., Zhou, S., Parworth, C., Zheng, B., Canonaco, F., Prévôt, A. S. H., Chen, P., Zhang, H., Wallington, T. J., and He, K.: Wintertime aerosol chemistry and haze evolution in an extremely polluted city of the North China Plain: significant contribution from coal and biomass combustion, Atmos. Chem. Phys., 17, 4751-4768, https://doi.org/10.5194/acp-17-4751-2017, 2017.

565 Li, J., Li, J., Wang, G., Zhang, T., Dai, W., Ho, K. F., Wang, Q., Shao, Y., Wu, C., and Li, L.: Molecular characteristics of organic compositions in fresh and aged biomass burning aerosols, Sci. Total Environ., 741, 140247, https://doi.org/10.1016/j.scitotenv.2020.140247, 2020.

Li, K., Zhang, J., Bell, D. M., Wang, T., Lamkaddam, H., Cui, T., Qi, L., Surdu, M., Wang, D., Du, L., El Haddad, I., Slowik, J. G., and Prevot, A. S. H.: Uncovering the dominant contribution of intermediate volatility compounds in secondary organic
570 aerosol formation from biomass-burning emissions, National Science Review,Natl. Sci. Rev., 11, https://doi.org/10.1093/nsr/nwae014, 2024.

Li, S., Zhang, H., Wang, Z., and Chen, Y.: Advances in the Research on Brown Carbon Aerosols: Its Concentrations, Radiative

Forcing, and Effects on Climate, Aerosol Air Qual. Res., 23, 220336, http://dx.doi.org/10.4209/aaqr.220336, 2023a.

Li, S., Liu, D., Wu, Y., Hu, K., Jiang, X., Tian, P., Sheng, J., Pan, B., and Zhao, D.: Aging effects on residential biomass burning emissions under quasi-real atmospheric conditions, Environ. Pollut., 337, 122615, https://doi.org/10.1016/j.envpol.2023.122615, 2023b.

Li, S., Liu, D., Kong, S., Wu, Y., Hu, K., Zheng, H., Cheng, Y., Zheng, S., Jiang, X., Ding, S., Hu, D., Liu, Q., Tian, P., Zhao, D., and Sheng, J.: Evolution of source attributed organic aerosols and gases in a megacity of central China, Atmos. Chem. Phys., 22, 6937-6951, https://doi.org/10.5194/acp-22-6937-2022, 2022a.

Li, X., Sun, N., Jin, Q., Zhao, Z., Wang, L., Wang, Q., Gu, X., Li, Y., and Liu, X.: Light absorption properties of black and brown carbon in winter over the North China Plain: Impacts of regional biomass burning, Atmos. Environ., 278, 119100, https://doi.org/10.1016/j.atmosenv.2022.119100, 2022b.

Lin, G., Penner, J. E., Flanner, M. G., Sillman, S., Xu, L., and Zhou, C.: Radiative forcing of organic aerosol in the atmosphere and on snow: Effects of SOA and brown carbon, J. Geophys. Res. Atmos., 119, 7453-7476, https://doi.org/10.1002/2013JD021186, 2014.

Lin, P., Laskin, J., Nizkorodov, S. A., and Laskin, A.: Revealing Brown Carbon Chromophores Produced in Reactions of Methylglyoxal with Ammonium Sulfate, Environ. Sci. Technol., 49, 14257-14266, https://doi.org/10.1021/acs.est.5b03608, 2015.

Liu, D., Li, S., Hu, D., Kong, S., Cheng, Y., Wu, Y., Ding, S., Hu, K., Zheng, S., Yan, Q., Zheng, H., Zhao, D., Tian, P., Ye, J., Huang, M., and Ding, D.: Evolution of Aerosol Optical Properties from Wood Smoke in Real Atmosphere Influenced by Burning Phase and Solar Radiation, Environ. Sci. Technol., 55, 5677-5688, https://doi.org/10.1021/acs.est.0c07569, 2021.

Ma, Y., Chen, C., Wang, J., Jiang, Y., Zheng, Z., Chen, H., and Zheng, J.: Evolution in physiochemical and cloud condensation nuclei activation properties of crop residue burning particles during photochemical aging, J. Environ. Sci., 77, 43-53, https://doi.org/10.1016/j.jes.2018.06.004, 2019.

Mao, J., Ren, X., Brune, W. H., Olson, J. R., Crawford, J. H., Fried, A., Huey, L. G., Cohen, R. C., Heikes, B., Singh, H. B., Blake, D. R., Sachse, G. W., Diskin, G. S., Hall, S. R., and Shetter, R. E.: Airborne measurement of OH reactivity during INTEX-B, Atmos. Chem. Phys., 9, 163-173, https://doi.org/10.5194/acp-9-163-2009, 2009.

Martinsson, Middlebrook J., Eriksson, A. C., Nielsen, I M., Bahreini, E., Malmborg, V. B., Ahlberg, E., Andersen, C., Lindgren, R., Nyström, Jimenez, J. L R., Nordin, E. Z., Brune, W. H., Svenningsson, B., Swietlicki, E., Boman, C., and Pagels, J. H.: Impacts Canagaratna, M. R.: Evaluation of Combustion Conditions and Photochemical Processing on Composition-Dependent Collection Efficiencies for the Light Absorption of Biomass Combustion Aerodyne Aerosol, Environ. Mass Spectrometer using Field Data, Aerosol Sci. Technol., 49, 14663-1467 46, 258-271, https://doi.org/10.1021/acs.est.5b03205, 2015 1080/02786826.2011.620041, 2012.

Ni, H., Tian, J., Wang, X., Wang, Q., Han, Y., Cao, J., Long, X., Chen, L. W. A., Chow, J. C., Watson, J. G., Huang, R.-J., and Dusek, U.: PM2.5 emissions and source profiles from open burning of crop residues, Atmos. Environ., 169, 229-237, https://doi.org/10.1016/j.atmosenv.2017.08.063, 2017.

Olson, M. R., Victoria Garcia, M., Robinson, M. A., Van Rooy, P., Dietenberger, M. A., Bergin, M., and Schauer, J. J.: Investigation of black and brown carbon multiple-wavelength-dependent light absorption from biomass and fossil fuel combustion source emissions, J. Geophys. Res. Atmos., 120, 6682-6697, https://doi.org/10.1002/2014JD022970, 2015.

Paatero, P. and Tapper, U.: Positive matrix factorization: A non-negative factor model with optimal utilization of error estimates of data values, Environmetrics, 5, 111-126, https://doi.org/10.1002/env.3170050203, 1994.

Park, S.-S., Sim, S. Y., Bae, M.-S., and Schauer, J. J.: Size distribution of water-soluble components in particulate matter emitted from biomass burning, Atmos. Environ., 73, 62-72, https://doi.org/10.1016/j.atmosenv.2013.03.025, 2013.

Park, S., Son, S.-C., and Lee, S.: Characterization, sources, and light absorption of fine organic aerosols during summer and winter at an urban site, Atmos. Res., 213, 370-380, https://doi.org/10.1016/j.atmosres.2018.06.017, 2018.

Park, S., Yu, G.-H., and Bae, M.-S.: Effects of combustion condition and biomass type on the light absorption of fine organic aerosols from fresh biomass burning emissions over Korea, Environ. Pollut., 265, 114841, https://doi.org/10.1016/j.envpol.2020.114841, 2020.

Pokhrel, R. P., Wagner, N. L., Langridge, J. M., Lack, D. A., Jayarathne, T., Stone, E. A., Stockwell, C. E., Yokelson, R. J., and Murphy, S. M.: Parameterization of single-scattering albedo (SSA) and absorption Ångström exponent (AAE) with EC / OC for aerosol emissions from biomass burning, Atmos. Chem. Phys., 16, 9549-9561, https://doi.org/10.5194/acp-16-9549-2016, 2016.

Qian, Y., Yasunari, T. J., Doherty, S. J., Flanner, M. G., Lau, W. K. M., Ming, J., Wang, H., Wang, M., Warren, S. G., and Zhang, R.: Light-absorbing particles in snow and ice: Measurement and modeling of climatic and hydrological impact, Adv. Atmos. Sci., 32, 64-91, https://doi.org/10.1007/s00376-014-0010-0, 2015.

Reyes, F., Vasquez, Y., Gramsch, E., Oyola, P., Rappenglück, B., and Rubio, M. A.: Photooxidation of Emissions from Firewood and Pellet Combustion Using a Photochemical Chamber, Atmosphere, 10, 575, https://doi.org/10.3390/atmos10100575, 2019.

Rivellini, L. H., Adam, M. G., Kasthuriarachchi, N., and Lee, A. K. Y.: Characterization of carbonaceous aerosols in Singapore: insight from black carbon fragments and trace metal ions detected by a soot particle aerosol mass spectrometer, Atmos. Chem. Phys., 20, 5977-5993, https://doi.org/10.5194/acp-20-5977-2020, 2020.

Saleh, R.: From Measurements to Models: Toward Accurate Representation of Brown Carbon in Climate Calculations, Curr. Pollution. Rep., 6, 90-104, https://doi.org/10.1007/s40726-020-00139-3, 2020.

Saleh, R., Marks, M., Heo, J., Adams, P. J., Donahue, N. M., and Robinson, A. L.: Contribution of brown carbon and lensing to the direct radiative effect of carbonaceous aerosols from biomass and biofuel burning emissions, J. Geophys. Res. Atmos., 120, 10,285-210,296, https://doi.org/10.1002/2015JD023697, 2015.

Saleh, R., Robinson, E. S., Tkacik, D. S., Ahern, A. T., Liu, S., Aiken, A. C., Sullivan, R. C., Presto, A. A., Dubey, M. K., Yokelson, R. J., Donahue, N. M., and Robinson, A. L.: Brownness of organics in aerosols from biomass burning linked to their black carbon content, Nat. Geosci., 7, 647-650, https://doi.org/10.1038/ngeo2220, 2014.

Schnitzler, E. G., Liu, T., Hems, R. F., and Abbatt, J. P. D.: Emerging investigator series: heterogeneous OH oxidation of primary brown carbon aerosol: effects of relative humidity and volatility, Environ. Sci.: Processes Impacts, 22, 2162-2171, https://doi.org/10.1039/D0EM00311E, 2020.

Sinha, P., Hobbs, P. V., Yokelson, R. J., Bertschi, I. T., Blake, D. R., Simpson, I. J., Gao, S., Kirchstetter, T. W., and Novakov, T.: Emissions of trace gases and particles from savanna fires in southern Africa, J. Geophys. Res. Atmos., 108, https://doi.org/10.1029/2002JD002325, 2003.

Sumlin, B. J., Pandey, A., Walker, M. J., Pattison, R. S., Williams, B. J., and Chakrabarty, R. K.: Atmospheric Photooxidation

Diminishes Light Absorption by Primary Brown Carbon Aerosol from Biomass Burning, Environ. Sci. Technol. Lett., 4, 540-545, https://doi.org/10.1021/acs.estlett.7b00393, 2017.

Sun, J., Zhi, G., Hitzenberger, R., Chen, Y., Tian, C., Zhang, Y., Feng, Y., Cheng, M., Zhang, Y., Cai, J., Chen, F., Qiu, Y., Jiang, Z., Li, J., Zhang, G., and Mo, Y.: Emission factors and light absorption properties of brown carbon from household coal combustion in China, Atmos. Chem. Phys., 17, 4769-4780, https://doi.org/10.5194/acp-17-4769-2017, 2017.

Sun, J., Zhang, Y., Zhi, G., Hitzenberger, R., Jin, W., Chen, Y., Wang, L., Tian, C., Li, Z., Chen, R., Xiao, W., Cheng, Y., Yang, W., Yao, L., Cao, Y., Huang, D., Qiu, Y., Xu, J., Xia, X., Yang, X., Zhang, X., Zong, Z., Song, Y., and Wu, C.: Brown carbon's emission factors and optical characteristics in household biomass burning: developing a novel algorithm for estimating the contribution of brown carbon, Atmos. Chem. Phys., 21, 2329-2341, https://doi.org/10.5194/acp-21-2329-2021, 2021.

Thamban, N. M., Tripathi, S. N., Moosakutty, S. P., Kuntamukkala, P., and Kanawade, V. P.: Internally mixed black carbon in the Indo-Gangetic Plain and its effect on absorption enhancement, Atmos. Res., 197, 211-223, https://doi.org/10.1016/j.atmosres.2017.07.007, 2017.

Tian, J., Wang, Q., Ma, Y., Wang, J., Han, Y., and Cao, J.: Impacts of biomass burning and photochemical processing on the light absorption of brown carbon in the southeastern Tibetan Plateau, Atmos. Chem. Phys., 23, 1879-1892, https://doi.org/10.5194/acp-23-1879-2023, 2023.

Tian, J., Chow, J. C., Cao, J., Han, Y., Ni, H., Chen, L. W. A., Wang, X., Huang, R., Moosmüller, H., and Watson, J. G.: A Biomass Combustion Chamber: Design, Evaluation, and a Case Study of Wheat Straw Combustion Emission Tests, Aerosol Air Qual. Res., 15, 2104-2114, https://doi.org/10.4209/aaqr.2015.03.0167, 2015.

Tian, J., Wang, Q., Ni, H., Wang, M., Zhou, Y., Han, Y., Shen, Z., Pongpiachan, S., Zhang, N., Zhao, Z., Zhang, Q., Zhang, Y., Long, X., and Cao, J.: Emission Characteristics of Primary Brown Carbon Absorption From Biomass and Coal Burning: Development of an Optical Emission Inventory for China, J. Geophys. Res. Atmos., 124, 1879-1893, https://doi.org/10.1029/2018JD029352, 2019.

Tuccella, P., Pitari, G., Colaiuda, V., Raparelli, E., and Curci, G.: Present-day radiative effect from radiation-absorbing aerosols in snow, Atmos. Chem. Phys., 21, 6875-6893, https://doi.org/10.5194/acp-21-6875-2021, 2021.

Ulbrich, I. M., Canagaratna, M. R., Zhang, Q., Worsnop, D. R., and Jimenez, J. L.: Interpretation of organic components from Positive Matrix Factorization of aerosol mass spectrometric data, Atmos. Chem. Phys., 9, 2891-2918, https://doi.org/10.5194/acp-9-2891-2009, 2009.

Wang, J., Ye, J., Liu, D., Wu, Y., Zhao, J., Xu, W., Xie, C., Shen, F., Zhang, J., Ohno, P. E., Qin, Y., Zhao, X., Martin, S. T., Lee, A. K. Y., Fu, P., Jacob, D. J., Zhang, Q., Sun, Y., Chen, M., and Ge, X.: Characterization of submicron organic particles in Beijing during summertime: comparison between SP-AMS and HR-AMS, Atmos. Chem. Phys., 20, 14091-14102, https://doi.org/10.5194/acp-20-14091-2020, 2020a.

Wang, Q., Zhou, Y., Ma, N., Zhu, Y., Zhao, X., Zhu, S., Tao, J., Hong, J., Wu, W., Cheng, Y., and Su, H.: Review of Brown Carbon Aerosols in China: Pollution Level, Optical Properties, and Emissions, J. Geophys. Res. Atmos., 127, e2021JD035473, https://doi.org/10.1029/2021JD035473, 2022.

Wang, X., Heald, C. L., Ridley, D. A., Schwarz, J. P., Spackman, J. R., Perring, A. E., Coe, H., Liu, D., and Clarke, A. D.: Exploiting simultaneous observational constraints on mass and absorption to estimate the global direct radiative forcing of black carbon and brown carbon, Atmos. Chem. Phys., 14, 10989-11010, https://doi.org/10.5194/acp-14-10989-2014, 2014.

Wang, X., Jacob, D. J., Eastham, S. D., Sulprizio, M. P., Zhu, L., Chen, Q., Alexander, B., Sherwen, T., Evans, M. J., Lee, B. H., Haskins, J. D., Lopez-Hilfiker, F. D., Thornton, J. A., Huey, G. L., and Liao, H.: The role of chlorine in global tropospheric chemistry, Atmos. Chem. Phys., 19, 3981-4003, https://doi.org/10.5194/acp-19-3981-2019, 2019.

Wang, Y., Hu, M., Xu, N., Qin, Y., Wu, Z., Zeng, L., Huang, X., and He, L.: Chemical composition and light absorption of carbonaceous aerosols emitted from crop residue burning: influence of combustion efficiency, Atmos. Chem. Phys., 20, 13721-13734, https://doi.org/10.5194/acp-20-13721-2020, 2020b.

Wong, J. P. S., Tsagkaraki, M., Tsiodra, I., Mihalopoulos, N., Violaki, K., Kanakidou, M., Sciare, J., Nenes, A., and Weber, R. J.: Atmospheric evolution of molecular-weight-separated brown carbon from biomass burning, Atmos. Chem. Phys., 19, 7319-7334, https://doi.org/10.5194/acp-19-7319-2019, 2019.

Wu, Y., Liu, D., Wang, J., Shen, F., Chen, Y., Cui, S., Ge, S., Wu, Y., Chen, M., and Ge, X.: Characterization of Size-Resolved Hygroscopicity of Black Carbon Containing Particle in Urban Environment, Environ. Sci. Technol., 53, 14212 14221, https://doi.org/10.1021/acs.est.9b05546, 2019.

Xie, M., Hays, M. D., and Holder, A. L.: Light-absorbing organic carbon from prescribed and laboratory biomass burning and gasoline vehicle emissions, Sci. Rep., 7, 7318, https://doi.org/10.1038/s41598-017-06981-8, 2017a.

Xie, M., Chen, X., Hays, M. D., Lewandowski, M., Offenberg, J., Kleindienst, T. E., and Holder, A. L.: Light Absorption of Secondary Organic Aerosol: Composition and Contribution of Nitroaromatic Compounds, Environ. Sci. Technol., 51, 11607-11616, https://doi.org/10.1021/acs.est.7b03263, 2017b.

Xu, W., Croteau, P., Williams, L., Canagaratna, M., Onasch, T., Cross, E., Zhang, X., Robinson, W., Worsnop, D., and Jayne, J.: Laboratory characterization of an aerosol chemical speciation monitor with PM2.5 measurement capability, Aerosol Sci. Technol., 51, 69-83, https://doi.org/10.1080/02786826.2016.1241859, 2017.

Yan, J., Wang, X., Gong, P., Wang, C., and Cong, Z.: Review of brown carbon aerosols: Recent progress and perspectives, Sci. Total Environ., 634, 1475-1485, https://doi.org/10.1016/j.scitotenv.2018.04.083, 2018.

Yang, Z., Tsona, N. T., George, C., and Du, L.: Nitrogen-Containing Compounds Enhance Light Absorption of Aromatic-Derived Brown Carbon, Environ. Sci. Technol., 56, 4005-4016, https://doi.org/10.1021/acs.est.1c08794, 2022.

Ye, C., Zhang, N., Gao, H., and Zhou, X.: Photolysis of Particulate Nitrate as a Source of HONO and NOx, Environ. Sci. Technol., 51, 6849-6856, https://doi.org/10.1021/acs.est.7b00387, 2017.

Ye, C., Zhou, X., Zhang, Y., Wang, Y., Wang, J., Zhang, C., Woodward-Massey, R., Cantrell, C., Mauldin, R. L., Campos, T., Hornbrook, R. S., Ortega, J., Apel, E. C., Haggerty, J., Hall, S., Ullmann, K., Weinheimer, A., Stutz, J., Karl, T., Smith, J. N., Guenther, A., and Song, S.: Synthesizing evidence for the external cycling of NOx in high- to low-NOx atmospheres, Nat. Commun., 14, 7995, https://doi.org/10.1038/s41467-023-43866-z, 2023.

Ye, Z., Qu, Z., Ma, S., Luo, S., Chen, Y., Chen, H., Chen, Y., Zhao, Z., Chen, M., and Ge, X.: A comprehensive investigation of aqueous-phase photochemical oxidation of 4-ethylphenol, Sci. Total Environ., 685, 976-985, https://doi.org/10.1016/j.scitotenv.2019.06.276, 2019.

Zanatta, M., Laj, P., Gysel, M., Baltensperger, U., Vratolis, S., Eleftheriadis, K., Kondo, Y., Dubuisson, P., Winiarek, V., Kazadzis, S., Tunved, P., and Jacobi, H. W.: Effects of mixing state on optical and radiative properties of black carbon in the European Arctic, Atmos. Chem. Phys., 18, 14037-14057, https://doi.org/10.5194/acp-18-14037-2018, 2018.

Zhang, L., Luo, Z., Du, W., Li, G., Shen, G., Cheng, H., and Tao, S.: Light absorption properties and absorption emission

factors for indoor biomass burning, Environ. Pollut., 267, 115652, https://doi.org/10.1016/j.envpol.2020.115652, 2020.

Zhang, Q., Jimenez, J. L., Canagaratna, M. R., Ulbrich, I. M., Ng, N. L., Worsnop, D. R., and Sun, Y.: Understanding atmospheric organic aerosols via factor analysis of aerosol mass spectrometry: a review, Anal. Bioanal. Chem., 401, 3045-3067, https://doi.org/10.1007/s00216-011-5355-y, 2011.

725   Zhao, R., Lee, A. K. Y., Huang, L., Li, X., Yang, F., and Abbatt, J. P. D.: Photochemical processing of aqueous atmospheric brown carbon, Atmos. Chem. Phys., 15, 6087-6100, https://doi.org/10.5194/acp-15-6087-2015, 2015.

Zhao, R., Zhang, Q., Xu, X., Wang, W., Zhao, W., Zhang, W., and Zhang, Y.: Effect of photooxidation on size distribution, light absorption, and molecular compositions of smoke particles from rice straw combustion, Environ. Pollut., 311, 119950, https://doi.org/10.1016/j.envpol.2022.119950, 2022.